Role of Microwave Heating Strategies in Enhancing the Progress of a First-Order Endothermic Reaction

Madhuchhanda Bhattacharya
C2-5-4C, Delhi Avenue, Indian Institute of Technology Madras Campus, Chennai 600036, India

Sandeep KR Venkata and Tanmay Basak
Dept. of Chemical Engineering, Indian Institute of Technology Madras, Chennai 600036, India

DOI 10.1002/aic.13848
Published online June 20, 2012 in Wiley Online Library (wileyonlinelibrary.com).

*A detailed analysis has been carried out by solving coupled energy and mass balance equations along with Helmholtz equation of microwave propagation to investigate the role of microwave heating strategies in enhancing the progress of a first-order endothermic reaction in "*thin*," "*intermediate*," and "*thick*" regimes of microwave heating. It has been shown that heating strategy plays a critical role in maximizing the efficiency of microwave heated reactors, where progress of reactor can be greatly accelerated at a given input power by either configuring microwave sources at both sides of the reactor or preferentially focusing them on one side. A series of master curves have been provided showing percentage saving of reaction time in various configurations of microwave heated reactors compared to their conventional counterparts, which can be efficiently used to select appropriate heating strategy for different dimension and dielectric properties of the reacting medium.* © 2012 American Institute of Chemical Engineers *AIChE J,* 59: 656–670, 2013
Keywords: transport, energy, heat transfer, mathematical modeling, numerical solution

Introduction

High frequency electromagnetic waves within the frequency band of 300 MHz–300 GHz are known to exhibit volumetric heating effect during their propagation through polar materials.[1] This range of electromagnetic waves is called microwave and associated heating is called microwave heating. Microwave heating results from the interaction of the dipoles of a polar material in presence of electromagnetic field. During the last few decades, microwave heating has gained significant popularity over the conventional heating in various fields on material processing[2–13] mainly due to its quick start up and shorter processing time. In the previous years, one of the major application of microwave heating has been in the area of material synthesis involving chemical reactions. Since reaction rates are highly dependent on local temperature, lower-temperature inside the reacting medium can limit the overall progress of reactions in conventional heating, where heat has to penetrate from the outer boundary of the reacting system. The situation can even worsen for endothermic reactions, which require continuous supply of heat to proceed. In these cases, microwave heating can be a better alternative due to its ability to speed up the progress of reaction by volumetrically supplying heat inside the reactor. This has been proved experimentally in numerous experimental investigations for various different classes of reactions, which can be found in a few extensive reviews.[14–34]

Correspondence concerning this article should be addressed to T. Basak at tanmay@iitm.ac.in.

Although previous investigations show accelerated progress of reaction under microwave heating, a quantitative understanding behind the observed enhancement of reaction rate is still lacking from these studies. This may be partly due to the difficulties in measuring local temperature within the reacting medium without which it is impossible to predict local enhancement of reaction rate. It may be noted that microwave heating can be highly nonuniform and lead to local hot spots depending on the configurations of the reacting system.[35–39] Local hot spots may cause dramatic enhancement of reaction rate locally and result in the observed acceleration of overall progress of reaction. In such cases, use of average temperature (as has been done in earlier works) may lead to speculation of athermal effect of microwave heating.[26,40,41] Thus, it is essential to consider the variations of temperature within the reacting medium, which may only be possible through a detailed mathematical model. A detailed mathematical model is also required to quantify the observed enhancement of reaction rate under various reacting conditions.

A few theoretical work has been conducted to study the interplay between microwave heating and reaction rate.[17,42–46] However, these studies assumed empirical model for microwave propagation, where induced electric field was assumed to be uniform while nonuniformity of microwave heating was introduced through variations of dielectric properties with temperature. Although these studies revealed the role of local hot spots in enhancing overall reaction rate, they lack quantitative analysis of microwave heating due to lack of detailed model for microwave propagation. For the same reason, earlier theoretical work missed out many important

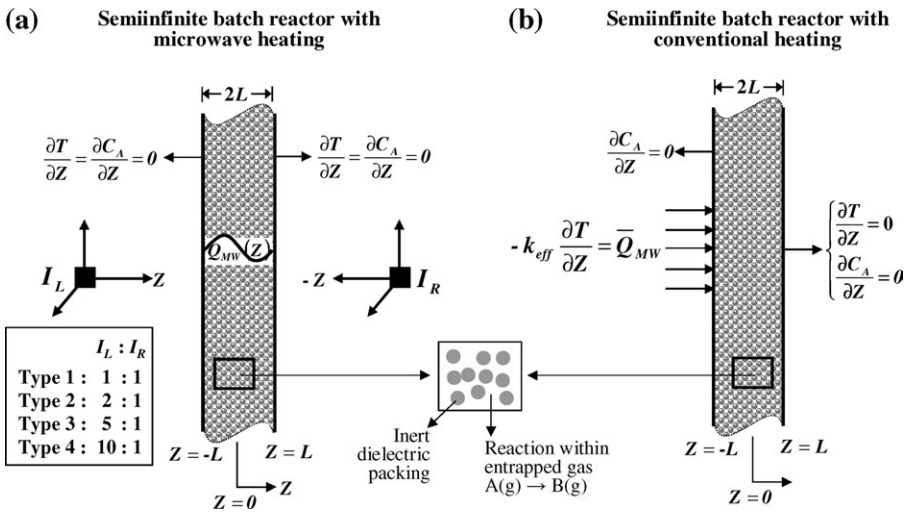

Figure 1. (a) Reactor configuration for microwave heating of varying incidence types denoted by Type 1–Type 4 configurations; (b) reactor configuration for equivalent conventional heating.

possibilities of microwave heating, where induced electric field can be highly oscillatory within the reacting medium leading to multiple local hot spots.[36–38] As local hot spots lead to the nontrivial enhancement of reaction rate, it is necessary to consider the detailed model for microwave propagation to quantify the effect of microwave heating on reaction rate under various configurations.

In this work, we consider detail description of microwave propagation in terms of Helmholtz equation, which can capture various possible patterns associated with microwave heating.[1] The effect of microwave heating is analyzed for a first-order endothermic reaction occurring in a semi-infinite vertical column. The column is assumed to be exposed to microwaves of varying intensities from left and right sides. It may be noted that intensity as well as distributions of microwave induced electric field within the reactor depend on the individual intensity of incident radiations from each side of the reactor. Variations of incident radiations from either side alter transmitted and reflected wave patterns, which in turn alter the resultant electric field within the reactor.[36–38] Thus, intensity as well as location of local hot spots can be altered by varying intensities of incident radiations on either left or right sides of the reactor. This leads to the primary objective of this work, which is to investigate optimal strategy of microwave heating to maximize the progress of reaction for a given reactor specifications. For this purpose, we have considered four different strategies of microwave heating, where different intensities of microwave sources are configured at left and right sides of the reactor keeping total input power constant. These configurations are selected in such a way that they represent the entire spectrum of microwave source arrangements starting from uniform radiations from both sides to highly localized radiations from one side.

As formation as well as intensity of transmitted and reflected waves also depend on the reactor dimension in addition to microwave source configuration and dielectric properties,[36–38] optimal strategy of microwave heating may also change with reactor dimension. Correspondingly, another objective of this work is to quantify the enhancement of reactor progress due to various configurations of microwave heating for the entire range of reactor dimensions related to microwave propagation. In this regard, a conventional reactor is designed for each configuration of microwave heating, where total amount of microwave power absorbed by the reactor is supplied as heat flux from the surface in its conventional counterpart. Simulations are carried out for both the modes of heating (microwave and conventional) to compare and quantify the enhancement of reactor progress due to microwave heating compared to conventional heating for different reactor dimensions and microwave heating strategies. The entire analysis is carried out by considering a detailed model including thermal and mass transport in addition to the complete description of microwave propagation.

Mathematical Formulation

Let us consider a semi-infinite batch reactor of width $2L$, where the entrapped gaseous species (A) is undergoing a homogeneous endothermic first-order reaction given by $\mathrm{A(g)} \xrightarrow{k_R} \mathrm{B(g)}$ (Figure 1). The heat required for the endothermic reaction is supplied by two different modes, namely (1) microwave and (2) conventional heating as shown in Figures 1a, b, respectively. As gases do not absorb microwave, the reactor is filled with inert dielectric packings, which absorb microwave energy and act as local heat sources under the exposure of microwave radiations (as shown in the zoomed portion in Figure 1). Here, dielectric packings play the role of susceptors and allow volumetric heating of the gas phase under microwave radiation. On the other hand, heat is supplied from left surface of the reactor in conventional heating (Figure 1b).

We have considered four different microwave heating strategies, where reactor is exposed to varying intensities of microwave radiations from left (I_L) and right (I_R) sides as I_L:I_R = 1:1, 2:1, 5:1, and 10:1. It may be noted that total intensity of incident radiation ($I_0 = I_L + I_R$) is maintained to be constant in all the cases. These heating configurations will be referred to as Type 1, Type 2, Type 3, and Type 4, respectively (as shown in Figure 1a). Type 1–Type 4 strategies span the entire possibility of microwave source configurations for this specific scenario. Type 1 considers equal intensity of microwave radiation from both sides. On the other hand, Type 4 resembles one side incidence, where microwave source is preferentially configured at left side. Intermediate Type 2 and Type 3 configurations simulate the

transition from both sides to one side incidence. It may be noted that, enhanced reactor progress under one sided microwave radiation ($I_L = I_0$) has recently been investigated in details for various regimes of microwave heating.[47] The main focus of this work is to investigate the role of microwave heating strategies for further enhancement of reactor progress and, thus, to examine the optimum heating strategies in different regimes of microwave heating.

For all the configurations, generalized formulation for microwave propagation and associated heat generation (Q_{MW}) within the semi-infinite packed reactor can be mathematically represented as[1]

$$Q_{MW}(E_x) = \frac{2\lambda_0 I_0}{\lambda_{eff} D_{p_{eff}}} E_x E_x^*, \tag{1}$$

where microwave induced electric field (E_x) and its conjugate (E_x^*) can be obtained from the following Helmholtz equations within free space-sample-free space assembly

$$\frac{d^2E_x}{dZ^2} + \left(\frac{2\pi}{\lambda_{eff}} + i\frac{1}{D_{p_{eff}}}\right)^2 E_x = 0, \quad -L \le Z \le L, \tag{2a}$$

$$\frac{d^2E_f}{dZ^2} + \frac{4\pi^2}{\lambda_0^2} E_f = 0, \quad Z < -L \text{ and } Z > L, \tag{2b}$$

along with continuity of electric and magnetic field at the sample-free space interfaces given by

$$@\, Z = \pm L : \left\{ E_x = E_f, \frac{dE_x}{dZ} = \frac{dE_f}{dZ}. \right. \tag{2c}$$

In the above equations, E_f is the microwave induced electric field within the surrounding free space on left and right sides of the reactor (between the reactor and the microwave sources), λ_{eff} and $D_{p_{eff}}$ are the effective wavelength and penetration depth of microwave within the packed bed,[48] respectively, and λ_0 is the wavelength of microwave within free space. (The expression for λ_{eff}, $D_{p_{eff}}$, and λ_0 are given in Appendix A.) The above equations have to be solved with the additional conditions of incident field intensities of $\sqrt{I_L/I_0}$ and $\sqrt{I_R/I_0}$ from left and right side, respectively. (Note that electric fields in Eqs. 1–2 are scaled with $\sqrt{2I_0/c\varepsilon_0}$, where c is the velocity of light and ε_0 is the free space permittivity.) It may be noted that Eqs. 2a–2c are based on spatial representations of Maxwell equations.[1] Alternatively, microwave propagation can also be represented as function of space as well as time, which can be solved by finite difference time domain method.[49–52] However, these two representations of wave propagation are equivalent and former form is adopted due to its simplicity.

With dielectric packing acting as local heat sources, evolution of temperature and reactant concentration (from uniform initial states of T_0 and C_{A_0}, respectively) in case of microwave heating can be obtained from the following governing equations and associated boundary and initial conditions

$$(\rho C_p)_{eff} \frac{\partial T}{\partial t} = k_{eff} \frac{\partial^2 T}{\partial Z^2} + Q_{MW} - \phi \Delta H_R R(C_A, T), \quad -L \le Z \le L \tag{3a}$$

$$\phi \frac{\partial C_A}{\partial t} = D_{eff} \frac{\partial^2 C_A}{\partial Z^2} - \phi R(C_A, T), \quad -L \le Z \le L \tag{3b}$$

$$@\, Z = \pm L : \left\{ \frac{\partial T}{\partial Z} = \frac{\partial C_A}{\partial Z} = 0. \right. \tag{3c}$$

$$@\, t = 0 : \{ T = T_0, C_A = C_{A_0}. \tag{3d}$$

These equations are based on the assumption of local thermal equilibrium and negligible convection within gas phase along with the assumption of heat/mass impermeable reactor walls. It is also assumed that diffusivity of product B is of same order of magnitude as that of reactant A and all thermal and physical properties are invariant of temperature/concentration. In addition, the reactor is further assumed to be homogeneously packed so that porosity (ϕ) becomes position invariant. In Eq. 3, $(\rho C_p)_{eff} = \phi(\rho C_p)_g + (1-\phi)(\rho C_p)_p$ and $k_{eff} = \phi k_g + (1-\phi)k_p$ are effective heat capacity and thermal conductivity of the packed bed, respectively, with subscripts g and p denoting gas phase and packing materials, respectively. In addition, $D_{eff} = D_A \phi/\tau_p$ with D_A as the molecular diffusivity of reactant and τ_p as the tortuosity of the porous bed is the effective diffusivity of reactant A, ΔH_R is the heat of reaction and $R(C_A, T)$ is the first-order homogeneous reaction rate, which obeys the following Arrhenius temperature dependency

$$R(C_A, T) = k_R C_A \exp\left[-\frac{E}{RT}\right]. \tag{4}$$

Here, k_R is the first-order rate constant, E is the activation energy and R is the universal gas constant.

Introducing the following dimensionless variables

$$z = \frac{Z+L}{2L}, \quad \tau = \frac{\alpha_{eff} t}{4L^2}, \quad \theta = \frac{k_{eff}(T-T_0)}{2LI_0},$$
$$c_A = \frac{C_A}{C_{A_0}}, \quad \tilde{E}_x(z) = E_x(L(2z-1)), \quad \tilde{E}_f(z) = E_f(L(2z-1)),$$
$$r(c_A, \theta) = \frac{R(C_A, T)}{R(C_{A_0}, T_0)}, \quad q_{MW} = \frac{2LQ_{MW}}{I_0} \tag{5}$$

the governing equations (Eqs. 2 and 3) can be rewritten in the following dimensionless form

$$\frac{\partial \theta}{\partial \tau} = \frac{\partial^2 \theta}{\partial z^2} + q_{MW}(\tilde{E}_x) - N_R r(c_A, \theta), \quad 0 \le z \le 1 \tag{6a}$$

$$\tau_D \frac{\partial c_A}{\partial \tau} = \frac{\partial^2 c_A}{\partial z^2} - \Phi_R r(c_A, \theta), \quad 0 \le z \le 1 \tag{6b}$$

$$\frac{d^2\tilde{E}_x}{dz^2} + 4\pi^2 N_w^2 (1 + i f_p)^2 \tilde{E}_x = 0, \quad 0 \le z \le 1 \tag{6c}$$

$$\frac{d^2\tilde{E}_f}{dz^2} + 4\pi^2 N_w^2 f_w^2 \tilde{E}_f = 0, \quad z < 0 \text{ and } z > 1 \tag{6d}$$

$$@\, z = 0, 1 : \left\{ \frac{\partial \theta}{\partial z} = \frac{\partial c_A}{\partial z} = 0, \tilde{E}_x = \tilde{E}_f, \frac{d\tilde{E}_x}{dz} = \frac{d\tilde{E}_f}{dz} \right. \tag{6e}$$

$$@\, \tau = 0 : \theta = 0, c_A = 1 \tag{6f}$$

The functional form of dimensionless absorbed power $[q_{MW}(z)]$ and reaction rate $[r(c_A, \theta)]$ are given by

$$q_{MW}(\tilde{E}_x) = \frac{4\pi N_w f_p}{f_w} \tilde{E}_x(z) \tilde{E}_x^*(z) \tag{7a}$$

and

$$r(c_A, \theta) = c_A \exp\left[\gamma_R \frac{\theta}{\theta + \beta}\right], \tag{7b}$$

with $\gamma_R = E/RT_0$ as the dimensionless activation energy.

In Eq. 6, a few dimensionless numbers have been introduced, which can be grouped into two different sets. The first set of dimensionless numbers given by N_w, f_w, and f_p are related to microwave propagation within the packed bed and are defined as

$$N_w = \frac{2L}{\lambda_{eff}}, \quad f_p = \frac{\lambda_{eff}}{2\pi D_{p_{eff}}}, \quad f_w = \frac{\lambda_{eff}}{\lambda_0}. \tag{8a}$$

Here, wave number (N_w), which is the ratio of reactor thickness to the wavelength of microwave, captures the effect of reactor thickness on microwave propagation. On the other hand, dimensionless numbers f_w and f_p capture the effect of varying dielectric properties of the packed bed via the ratio of λ_{eff} to λ_0 and λ_{eff} to $2\pi D_{p_{eff}}$, respectively. The second set of dimensionless numbers in Eq. 6 are related to thermal and reactant transport within the reactor and are defined as

$$\Phi_R = \frac{4L^2 \phi R(C_{A_0}, T_0)}{D_{eff} C_{A_0}}, \quad \beta = \frac{k_{eff} T_0}{2LI_0},$$
$$\tau_D = \frac{\phi \alpha_{eff}}{D_{eff}}, \quad N_R = \frac{2L\Delta H_R \phi R(C_{A_0}, T_0)}{I_0}. \tag{8b}$$

The above numbers represent the ratios of various transport time scales and in turn measure the thermal/reactant transport resistances within the reactor. Bulk Thiele modulus (Φ_R) represents the ratio of diffusion time ($4L^2/D_{eff}$) to homogeneous reaction time within gas phase ($C_{A_0}/\phi R(C_{A_0}, T_0)$) and is a measure of mass-transfer resistance within the reactor. Similarly, heat-transfer resistance within the reactor is represented by conduction number (β), which is a relative measure of heating time ($(\rho C_p)_{eff} T_0/(I_0/2L)$) compared to thermal diffusion time ($4L^2(\rho C_p)_{eff}/k_{eff}$). The relative speed of thermal and reactant diffusion within the reactor is measured by diffusion number (τ_D), which represents the ratio of mass diffusion time ($4L^2/D_{eff}$) to thermal diffusion time ($4L^2/\alpha_{eff}$). Since the reaction is endothermic, an important aspect of reactor analysis is the relative rate of heat required by reaction ($\Delta H_R \phi R(C_{A_0}, T_0)$) compared to the rate at which heat is supplied to the reactor ($I_0/2L$). This is denoted as heat-reaction number (N_R) in this work.

It may be noted that governing equation for concentration (Eq. 3b) is invariant of the mode of heating and, thus, remains unchanged for conventional reactor. However, energy balance equation (Eq. 3a) and associated thermal boundary conditions modify with the modes of heating. For the configuration of conventional heating considered in Figure 1b, Eq. 3a modifies to

$$(\rho C_p)_{eff} \frac{\partial T}{\partial t} = k_{eff} \frac{\partial^2 T}{\partial Z^2} - \phi \Delta H_R R(C_A, T) \tag{9a}$$

and surface heating of reactor is incorporated via thermal boundary condition at $Z = -L$ as

$$-k_{eff} \frac{\partial T}{\partial Z} = \int_{-L}^{L} Q_{MW} dZ. \tag{9b}$$

The right boundary of the reactor remains thermally insulated as in case of microwave heating. It may be noted that $\int_{-L}^{L} Q_{MW} dZ$ is the total power absorbed by the packed column in microwave mode of heating. Thus, Eq. 9b ensures equal heating rate in the two modes of heating to make them comparable. In terms of dimensionless variables and dimensionless numbers, the dimensionless governing equations for conventional reactor can be written as

$$\frac{\partial \theta}{\partial \tau} = \frac{\partial^2 \theta}{\partial z^2} - N_R r(c_A, \theta) \tag{10a}$$

$$\tau_D \frac{\partial c_A}{\partial \tau} = \frac{\partial^2 c_A}{\partial z^2} - \Phi_R r(c_A, \theta) \tag{10b}$$

$$@\tau = 0 : \{\theta = 0, c_A = 1 \tag{10c}$$

$$@z = 0 : \begin{cases} -\frac{\partial \theta}{\partial z} = \bar{q}_{MW}, \frac{\partial c_A}{\partial z} = 0 \end{cases} \tag{10d}$$

$$@\, z = 1 : \begin{cases} \frac{\partial \theta}{\partial z} = \frac{\partial c_A}{\partial z} = 0 \end{cases} \tag{10e}$$

where dimensionless surface heat flux for conventional heating $\bar{q}_{MW} = \int_0^1 q_{MW} dz$ is also equal to dimensionless average absorbed power in Type 1–Type 4 microwave heating configurations.

Solution Strategy

According to the formulation of Eqs. 6c–6e, determination of q_{MW} involves computation of $\tilde{E}_f$ (from Eq. 6d) within the large domain of surrounding free space outside the reactor. This may increase the computational cost significantly for simulation of reactor progress especially for temperature dependent dielectric properties, where q_{MW} has to be evaluated at each time step. To reduce the computational cost, evaluation of $\tilde{E}_f$ can be avoided by expressing it[53,54] as

$$\tilde{E}_f = \begin{cases} \sqrt{\frac{I_L}{I_0}} \exp[2\pi N_w f_w i(z - 1/2)] + A_L \exp[-2\pi N_w f_w i(z - 1/2)] & \forall z < 0 \\ A_R \exp[2\pi N_w f_w i(z - 1/2)] + \sqrt{\frac{I_R}{I_0}} \exp[-2\pi N_w f_w i(z - 1/2)] & \forall z > 1 \end{cases} \tag{11}$$

where A_L and A_R can be determined in terms of $\tilde{E}_x(z = 0)$ and $\tilde{E}_x(z = 1)$, respectively from the continuity of electric field at sample-free space interfaces ($\tilde{E}_x = \tilde{E}_f$ at $z = 0$ and 1). Subsequently, $d\tilde{E}_f/dz$ can be expressed in terms of $\tilde{E}_x(z = 0)$ and $\tilde{E}_x(z = 1)$, which when substituted in the interfacial flux continuity conditions for electric field ($d\tilde{E}_x/dz = d\tilde{E}_f/dz$) leads to the following conditions involving only $\tilde{E}_x$:

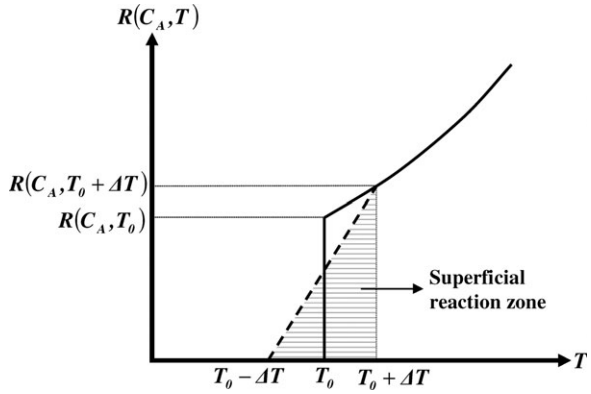

Figure 2. Schematic representation of superficial reaction zone.

$$@\, z = 0 : \frac{d\tilde{E}_x}{dz} + i2\pi N_w f_w \tilde{E}_x = i4\pi N_w f_w \sqrt{\frac{I_L}{I_0}} \exp[-i\pi N_w f_w] \tag{12a}$$

$$@\, z = 1 : \frac{d\tilde{E}_x}{dz} - i2\pi N_w f_w \tilde{E}_x = -i4\pi N_w f_w \sqrt{\frac{I_R}{I_0}} \exp[-i\pi N_w f_w], \tag{12b}$$

which are called radiation boundary conditions for electric field.[35,53] It may be noted that Eq. 12 captures incidence, transmission, and reflection of electromagnetic wave at the sample boundaries considered via free space wave propagation and interface continuity conditions in Eqs. 6d and 6e in free space-sample-free space assembly representation. Thus, electric field within the reactor and the resulting heating profile can be equivalently determined by considering only the reactor and solving Eq. 6c with modified boundary conditions given by Eq. 12. This approach eliminates the necessity of solving Eq. 6d within the surrounding free spaces and, thus, allows to solve the energy and mass balance equations (Eqs. 6a and 6b) simultaneously with electric field equations (Eqs. 6c and 12). It may be noted that analytical solution for electric field and associated heating profiles can be obtained for constant dielectric properties[54,55] and are given by

$$q_{MW} = \frac{16\pi N_w f_w f_p}{C^d}[C_1^n \cosh(2\pi N_w f_p(2z-1)) + C_2^n \sinh(2\pi N_w f_p(2z-1)) + C_3^n \cos(2\pi N_w(2z-1)) + C_4^n \sin(2\pi N_w(2z-1))], \tag{13}$$

where coefficients C_1^n–C_4^n and C^d are functions of N_w, f_w, f_p, and microwave source configuration (I_L/I_0 and I_R/I_0) as reported in Appendix B. The closed form solution of q_{MW} can be directly used in Eqs. 6a and 6b to simulate the reactor dynamics. However, numerical solution of Eq. 6c along with Eq. 12 in conjunction with Eqs. 6a and 6b are more generic and is carried out in this work to simulate reactor dynamics in presence of microwave heating using the numerical procedure as described below.

It is important to note that simulation of endothermic reaction may result in unrealistic temperature drop within the reactor if the reaction is not stopped below a critical temperature. Correspondingly, we have stopped the reaction once local temperature reduces beyond T_0 during the simulation. As a result, simulated reaction rate encounters a step jump given by

$$r(c_A, \theta) = \begin{cases} c_A \exp\left[\gamma_R \frac{\theta}{\theta+\beta}\right] & \text{for } \theta \geq 0 \\ 0 & \text{otherwise} \end{cases}, \tag{14}$$

and in turn poses numerical difficulties as discussed in literature for time tracing of a step jump.[56] (Figure 2 shows the typical step jump of the simulated reaction rate in solid line.) Accordingly, the step jump has been smoothed out by introducing a superficial reaction zone of width $2\Delta T$ around point of jump (shaded area of Figure 2). (This is similar to the superficial phase change region assumed in the simulation of solidification/melting of pure phase change problem.[56]) Within the superficial reaction zone, reaction rate is assumed to increase linearly from 0 at $T = T - \Delta T$ to $R(C_A, T_0 + \Delta T)$ at $T = T_0 + \Delta T$ as shown by dotted lines in Figure 2. Beyond the superficial reaction zone ($T \geq T_0 + \Delta T$), reaction rate follows the actual exponential variation with temperature. The modified reaction rate with the inclusion of superficial reaction zone can be mathematically represented in terms of dimensionless concentration and temperature as

$$\hat{r}(c_A, \theta) = \begin{cases} 0 & \text{for } \theta \leq -\varepsilon \\ r(c_A, \varepsilon)\left[\frac{\theta}{2\varepsilon} + \frac{1}{2}\right] & \text{for } -\varepsilon \leq \theta \leq \varepsilon \\ r(c_A, \theta) & \text{for } \theta > \varepsilon \end{cases} \tag{15}$$

where $\varepsilon = k_{eff}\Delta T/2LI_0$ is the dimensionless half width of the superficial reaction zone. It is obvious that $\hat{r}(c_A, \theta)$ approaches actual reaction rate ($r(c_A, \theta)$) in the limit of $\varepsilon \to 0$. In this work, we have used $\varepsilon = 10^{-5}$. The accuracy of the solutions with $\varepsilon = 10^{-5}$ are shown in Figure 3, which shows the

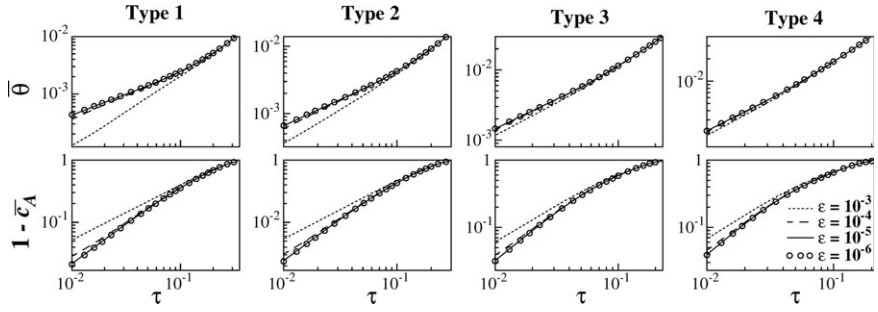

Figure 3. Convergence of numerical simulations ($\bar{\theta}$ and $1 - \bar{c}_A$ vs. τ) with respect to the width of superficial reaction zone ($\varepsilon = 10^{-3}$, 10^{-4}, 10^{-5}, and 10^{-6} in dotted, dash, solid lines, and circles, respectively) for conventional heating corresponding to Type 1–Type 4 configurations at $N_w = 0.5$, $f_p = 0.1$, $f_w = 0.1$, and $\Phi_R = 10$.

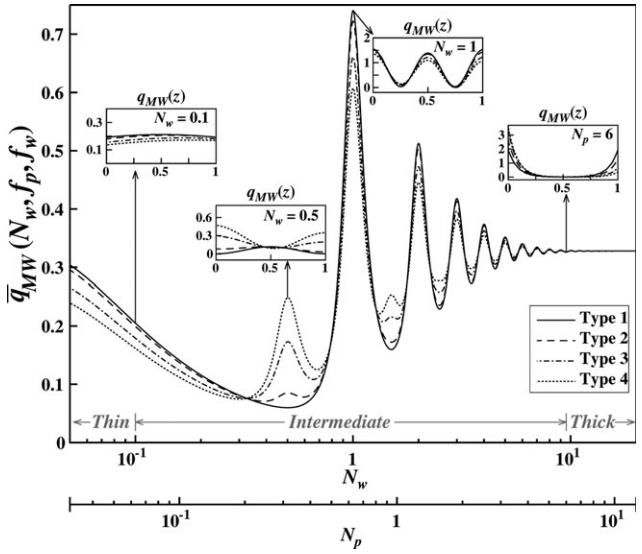

Figure 4. Effect of source configuration on intensity of power absorption ($\bar{q}_{MW}$) and absorbed power distribution in thin, intermediate, and thick regimes for $f_p = 0.1$ and $f_w = 0.1$ with solid, dash, dash-dotted, and dotted lines representing Type 1, Type 2, Type 3, and Type 4 configurations, respectively.

sensitivity of reactor simulations in terms of evolution of average reactant concentration ($\bar{c}_A = \int_0^1 c_A(z)dz$) and temperature ($\bar{\theta} = \int_0^1 \theta(z)dz$) for various ε as $\varepsilon = 10^{-3}$, 10^{-4}, 10^{-5}, and 10^{-6}. It may be noted that simulations of Figure 3 correspond to conventional reactor with intensity of heating equivalent to $N_w = 0.5, f_w = 0.1, f_p = 0.1$ and other parameters as $\Phi_R = 10, N_R = 0.1$, $\tau_D = 1.0$, $\beta = 0.1$, and $\gamma_R = 10$. Here, the simulations are shown for only conventional reactor since the surface heating results in much stiffer variation of reaction rate compared to its microwave counterparts. Figure 3 shows the sensitivity of simulations for various intensity of heating corresponding to Type 1–Type 4 incidences. It may be noted that numerical simulations become invariant of the width of the superficial reaction zone beyond $\varepsilon = 10^{-5}$ and, thus, we have used $\varepsilon = 10^{-5}$ in all the simulations.

Replacing $r(c_A, \theta)$ by $\hat{r}(c_A, \theta)$, Eqs. 6a–6c with associated radiation boundary conditions of electric field (Eq. 12) and no heat/mass flux ($d\theta/dz = dc_A/dz = 0$ at $z = 0, 1$) boundary conditions are spatially discretized using Galerkin finite element method[57] and time integrated using Crank-Nicholson scheme following the same procedure as described in an earlier work[47] to simulate reactor progress with microwave heating. It may be noted that electric field ($\tilde{E}_x$) has been computed in terms of its real ($\tilde{v}_x$) and imaginary ($\tilde{w}_x$) components and hence absorbed power is evaluated as $q_{MW} = 4\pi N_w f_p(\tilde{v}_x^2 + \tilde{w}_x^2)/f_w$. Here, we just mention that we have used 50 quadratic elements corresponding to 101 nodes across the width of the reactor and a dimensionless time step of $\Delta\tau = 0.0001$ for time integration. Also, we have used Galerkin weak formulation and evaluated the required Galerkin projections by three point Gaussian quadrature. The same numerical scheme has also been applied to Eq. 10 for simulation of conventionally heated reactor progress. All the simulations are stopped when minimum conversion within the reactor reaches 10%, which correspond to max (c_A) = 0.1. The time required for achieving this conversion will be denoted by reaction time or τ_f in the following discussion.

Result and Discussions

Occurrence of endothermic reaction strongly depends on availability of heat. Correspondingly, localized supply of heat from the surface limits the progress of reaction within conventional reactor in presence of heat and/or mass transfer limitations. In such cases, microwave heating enhances overall progress of reactor by providing heat and facilitating reaction in no/low reaction zones of conventional reactor. It follows that optimum utilization of microwave depends on spatial distribution of absorbed power ($q_{MW}(z)$), which in turn depends on width and dielectric properties of the reactor in addition to the microwave source configurations. These effects are captured by the dimensionless numbers N_w, f_w, f_p, and I_L/I_0 (since $I_R/I_0 = 1 - I_L/I_0$ for constant I_0) in Eqs. 6c and 12. It may be mentioned that another dimensionless number is commonly used in describing the microwave power absorption,[36] which is the ratio of the thickness of the sample to the penetration depth of microwave within it. This dimensionless number is called as penetration number or N_p and can be correlated to N_w and f_p by $N_p = 2L/D_{p_{eff}} = 2\pi N_w f_p$ (see Eq. 8a). Details of the effects of these dimensionless numbers on microwave power absorption have already been discussed in earlier work.[37,38] Here, we briefly discuss various possible absorbed power distributions and the effect of Type 1–Type 4 configurations on them.

Thin, intermediate, and thick regimes of microwave power absorption

Various possible absorbed power distributions can be classified into three different types, namely (1) uniform, (2) oscillatory or sinusoidal, and (3) exponentially attenuated distributions.[37,38] These distributions appear in three different range of reactor thickness and divide the entire range into (1) "thin," (2) "intermediate," and (3) "thick" regimes with respect to microwave power absorption.[37,38] Uniform absorption of microwave power occurs in thin regime, where thickness of the reactor is much lower than the wavelength of microwave within it ($2L \ll \lambda_{eff}/2$ or $N_w \ll 0.5$). On the other hand, exponentially attenuated absorbed power distributions occur in thick regime, where $2L$ is much greater than the penetration depth of microwave within it, that is, $2L \gg D_{p_{eff}}$ or $N_p \gg 1$. It has been shown in earlier work[37,38] that exponentially attenuated power distributions occur at $N_p \geq 6$ (or $N_w \geq 6/2\pi f_p$) if microwave sources are configured at both sides as in Type 1–Type 4 configurations. (The range of thick regime shifts to $N_p \geq 3$ for one-sided incidence, where either $I_L = 0$ or $I_R = 0$). Since $\lambda_{eff}/2 \leq \pi D_{p_{eff}}$ (see Eq. A1), there exists an intermediate demarcation zone in between thin and thick regimes, whose width depends on the magnitude of f_p. In intermediate regime, where thickness of the reactor is bounded by $0.5 \leq N_w \ll 6/2\pi f_p$ or $\pi f_p \leq N_p \ll 6$, absorbed power exhibits spatial oscillations due to destructive/constructive interference depending on the magnitude of N_w.[37,38]

Existence of three distinct regimes of microwave power absorption with respect to reactor thickness for Type 1–Type 4 microwave source configurations is illustrated in Figure 4 via few illustrative power distributions in thin ($N_w = 0.1$), intermediate ($N_w = 0.5$ and 1), and thick ($N_p = 6$) regimes at $f_p = f_w = 0.1$ (see the insets). Figure 4 also illustrates variations of $\bar{q}_{MW}$ from thin to thick regimes for all the configurations, where solid, dashed, dash-dotted, and dotted lines

represent Type 1, Type 2, Type 3, and Type 4 configurations, respectively. It may be noted that $\bar{q}_{MW}$ determines the intensity of surface heating (see Eq. 10) and play a critical role in determining the efficiency of microwave heating. It may be further noted that selection of $f_p = 0.1$ and $f_w = 0.1$ in Figure 4 is to illustrate all the three regimes of microwave power absorption since existence of intermediate regime depends on the magnitude of f_p[37,38] as will be illustrated later.

Figure 4 illustrates that source configuration does not alter absorbed power distribution but alters the intensity of power absorption ($\bar{q}_{MW}$) in thin regime. It may be noted that all the configurations lead to uniform power absorption in thin regime (see the inset for $N_w = 0.1$), where Type 1 configuration maximizes the intensity of microwave heating. On the other hand, power absorption pattern depends strongly on source configuration but total absorbed power ($\bar{q}_{MW}$) remains invariant in thick regime of microwave heating as may be observed from Figure 4. Microwave power absorption occurs from the surface in proportion to the intensity of source at the respective side and attenuates exponentially in thick regime of microwave heating. This causes highly intensified power absorption from one side (left surface) in Type 4 configuration compared to the equal power absorption from both sides in Type 1 configuration (see the inset for $N_p = 6$). Main characteristic of thick regime is penetration of microwave power only near the surface, which further shrinks with increasing sample width. As a result, microwave heating tends toward surface heating either from one or from both sides in the limit of $N_p \to \infty$.

In contrast to the previous two regimes, microwave source configuration influences both the intensity as well as pattern of power absorption in intermediate regime as illustrated in Figure 4 (see the absorbed power profiles for $N_w = 0.5$ and 1). Power absorption in intermediate regime is mainly governed by the constructive/destructive interference between oppositely traveling transmitted and reflected waves, which are formed due to transmission and reflection of incident field at the sample boundaries.[1,36,38] As a result, intermediate regime exhibits much pronounced dependencies on incident field orientation (Type 1–Type 4 configurations) compared to the other two regimes as observed in Figure 4 for $\bar{q}_{MW}$ as well as power distributions at $N_w = 0.5$ and 1. Typical characteristic of intermediate regime is the oscillatory power absorption in terms of both q_{MW} and $\bar{q}_{MW}$, which result from resonances of the induced field at the location of constructive interferences. It may be noted that $\bar{q}_{MW}$ exhibits resonances at $N_w = 1, 2, 3\ldots$ irrespective of source configuration with additional resonating peaks appearing at $N_w = 0.5, 1.5..$ as microwave source is configured from both side to one side with Type 1–Type 4 configurations (see in Figure 4). As a result, Type 4 configuration enhances microwave power absorption at source specific resonating locations of $N_w = 0.5, 1.5\ldots$. In contrast, Type 1 configuration results in higher power absorption at common resonating locations of $N_w = 1, 2..$ as may be observed from Figure 4. Source configurations also influence power distributions differently at common and source specific resonating locations. It is seen from Figure 4 that absorbed power distributions differ greatly from Type 1 to Type 4 configuration at the source specific resonating locations ($N_w = 0.5$), while they follow similar patterns for all the configurations at common resonating locations ($N_w = 1$).

It follows that source configuration either alters power distribution or influences intensity of power absorption, which are the two critical parameters in determining progress of reactor. Thus, selection of source configuration is expected to play a critical role in optimizing the efficiency microwave heating in enhancing reactor progress. A detailed analysis on the effect of Type 1–Type 4 configurations on various aspects of reactor dynamics will be presented and compared with conventional heating in the following section to determine optimum source configuration in thin, intermediate, or thick regimes.

Effect of microwave source configurations on dynamics and efficiency of microwave assisted reactor in thin, intermediate and, thick regimes of microwave heating

Enhanced reactor progress under microwave heating results from its homogenized heating pattern, which facilitates reaction in a greater portion of the reactor compared to its conventional counterpart. Reactants diffuse a greater distance from cold right wall to hot left wall to avail the supplied heat and react in case of conventional heating compared to the volumetric heating of microwave radiation. Thus, conventional heating results in a longer delay between supply and availability of heat for the reaction than microwave heating and causes slower reactor progress. However, reactant can avail the heat instantaneously even in the case of conventional heating if reactant can diffuse to the heating zone at a faster rate than its consumption rate and causes the reactor dynamics to be invariant of heating mode. Correspondingly, efficiency of a given microwave heating in enhancing the reactor progress depends on relative rate of diffusion compared to its consumption rate, which is measured by Thiele modulus (Φ_R) in this work (see Eq. 8b). This directed to analyze the efficiency of various configurations of thin, intermediate, and thick regime of microwave heating in two limiting cases of $\Phi_R \ll 1$ and $\phi_R \gg 1$. The former is known as kinetically controlled regime, while the later is called mass transfer controlled regime.

Other parameters considered in the simulations are $N_R = 0.1$, $\tau_D = 1$, $\beta = 0.1$, and $\gamma_R = 10$. Selection of these parameters is based on an earlier work[47] and justifications are summarized below for the brevity of the paper. Heat-reaction number has been selected to be lower than 1 ($N_R = 0.1$) to ensure enough supply of heat than that required by reaction, while equal thermal and reactant diffusivities at $\tau_D = 1$ has been selected to eliminate the influence of preferential diffusion of either mass or heat on the reactor performance. On the other hand, higher thermal diffusion time than the heating time at $\beta = 0.1$ retains the imposed thermal gradients of microwave and conventional heating to a reasonable extent, which is required to simulate the distinct effect of microwave heating on reactor performance.[47] It may be noted that supplied heat spreads uniformly across the reactor and results in uniform heating of the reactor irrespective of microwave or conventional heating if thermal diffusion is instantaneous compared to the heating rate ($\beta \gg 1$).

Effect of microwave source configurations on microwave assisted and conventional reactor dynamics in thin regime of power absorption ($N_w = 0.1$)

Figure 5 illustrates the effect of source configuration on the dynamics of thin regime of microwave assisted reactors (indicated by MW) in kinetically controlled ($\Phi_R = 0.1$) and mass transfer controlled regime ($\Phi_R = 10$) for $N_w = 0.1$, f_p

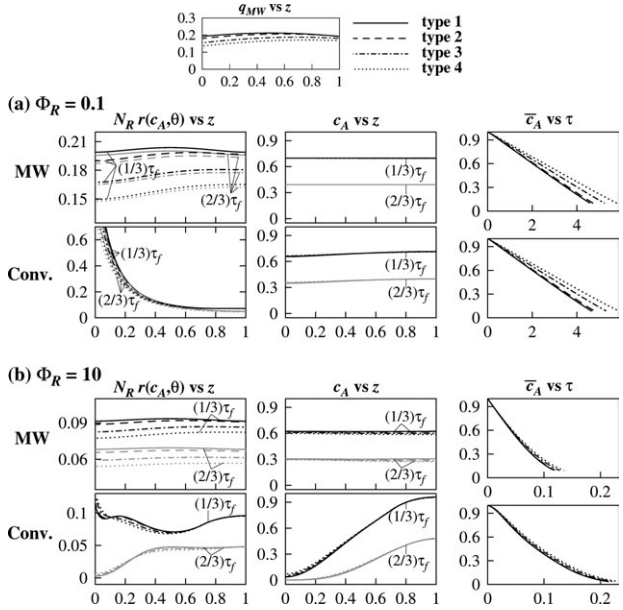

Figure 5. Spatial dynamics of reactor (shown at $\tau_f/3$ and $2\tau_f/3$ using darker and lighter shades, respectively) and overall reactor progress ($\bar{c}_A$ vs. τ) under microwave (MW) and conventional (Conv.) heating of Type 1–Type 4 configurations (solid, dash, dash-dotted, and dotted lines) in thin regime corresponding to $N_w = 0.1$, $f_p = 0.1$, and $f_w = 0.1$ for two limiting cases of $\Phi_R = 0.1$ and 10 in subplots (a) and (b), respectively.

$= 0.1$, and $f_w = 0.1$, where solid, dashed, dash-dotted, and dotted lines represent Type 1, Type 2, Type 3, and Type 4 configurations, respectively. Figure 5 also shows the dynamics of corresponding conventional reactors (indicated by Conv) for comparative analysis. Variations of absorbed power profiles with source configuration are also shown at the top. Here, reactor dynamics are compared in terms of concentration gradients (c_A vs. z) as well as overall reactor progress ($\bar{c}_A$ vs. τ). Reaction patterns within the reactors are also shown in terms of spatial heat requirement ($N_R r(c_A, \theta)$) for ease of illustrations. It may be noted that the spatial profiles are shown at two intermediate stages ($\tau_f/3$ and $2\tau_f/3$ using darker and lighter shades, respectively).

Following uniform power absorption, reaction in thin microwave assisted reactors occur almost uniformly for all the source configurations as reflected in the corresponding $N_R r(c_A, \theta)$ profiles for $N_w = 0.1$ in Figures 5a, b. Consequently, reactant concentration also remains uniform throughout the reaction irrespective of either Thiele modulus or source configurations at $N_w = 0.1$ (Figures 5a, b). In contrast, reaction is always localized near the hot (left) surface in case of conventional reactor causing its dynamics to be dependent on Thiele modulus. Dynamics of conventional reactor follow those of their microwave counterparts at $\Phi_R = 0.1$, where faster diffusion of reactant homogenizes the concentration gradients caused by nonuniform reaction. As a result, uniform reactant concentration prevails within conventional reactor in spite of its nonuniform reaction pattern (Figure 5a). Overall progress of reactor also remains invariant of the heating modes at $\Phi_R = 0.1$ as reflected in the $\bar{c}_A$ vs. τ diagrams of Type 1–Type 4 configurations. On the other hand, conventional heating leads to significantly different reactor dynamics at $\Phi_R = 10$, where reactant builds up near the cold right wall following its faster consumption near the localized heat source at left wall (Figure 5b). Correspondingly, microwave heating shows enhanced reactor progress for all the configurations in $\bar{c}_A$ vs. τ diagrams of Figure 5b at $\Phi_R = 10$.

Reaction time required for various configurations of conventional ($\tau_{f_{conv}}$) and microwave ($\tau_{f_{MW}}$) heating at $N_w = 0.1$ are reported in Table 1 for $\Phi_R = 0.1$ and 10, which reflect the features discussed above. It may be noted that Type 1 configuration maximizes savings of reaction time in thin regime as reflected in Table 1 for $N_w = 0.1$, which is due to higher intensity of $\bar{q}_{MW}$ and consequent increase in localization of reaction with conventional reactor corresponding to Type 1 configuration compared to other source configurations.

Effect of microwave source configurations on microwave assisted and conventional reactor dynamics in intermediate *regime of power absorption (N_w = 0.5 and 1)*

Effect of source configuration on the dynamics of reactors in intermediate regime are analyzed at the first source specific resonating peak ($N_w = 0.5$) as well as at the first common resonating peak ($N_w = 1$) representing two extreme scenarios (see discussion of "thin, intermediate, and thick regimes of microwave power absorption") and the results are shown in Figures 6 and 7, respectively, using the same format as in Figure 5. Figures 6 and 7 also present the results for $\Phi_R = 0.1$ and 10 in subplots (a) and (b), respectively, with other parameters remaining same as in Figure 5.

It follows from the illustrations of "thin, intermediate, and thick regimes of microwave power absorption" that reactor width or N_w plays an important role in determining the reaction patterns and their dependence on source configuration in

Table 1. Reaction Times under Type 1–Type 4 Configurations of Microwave Heating ($\tau_{f_{MW}}$) and Corresponding Conventional Heating ($\tau_{f_{Conv}}$) for Different Reactor Dimensions (N_w and N_p) in *Thin*, *Intermediate*, and *Thick* Regimes with $f_p = 0.1$, $f_w = 0.1$, and $\Phi_R = 0.1$ and 10

		$N_w = 0.1$		$N_w = 0.5$		$N_w = 1$		$N_p = 6$	
	$\Phi_R \rightarrow$	0.1	10	0.1	10	0.1	10	0.1	10
Type 1	$\tau_{f_{MW}}$	4.586	0.116	15.377	0.229	1.310	0.054	2.920	0.102
	$\tau_{f_{Conv}}$	4.661	0.215	15.406	0.335	1.429	0.149	3.004	0.187
Type 2	$\tau_{f_{MW}}$	4.719	0.119	10.86	0.195	1.345	0.056	2.938	0.107
	$\tau_{f_{Conv}}$	4.792	0.217	10.894	0.290	1.460	0.150	3.003	0.187
Type 3	$\tau_{f_{MW}}$	5.240	0.128	5.426	0.134	1.472	0.061	2.970	0.129
	$\tau_{f_{Conv}}$	5.308	0.224	5.485	0.227	1.579	0.154	3.001	0.187
Type 4	$\tau_{f_{MW}}$	5.793	0.135	3.803	0.110	1.600	0.065	2.982	0.147
	$\tau_{f_{Conv}}$	5.857	0.232	3.876	0.202	1.701	0.157	2.999	0.187

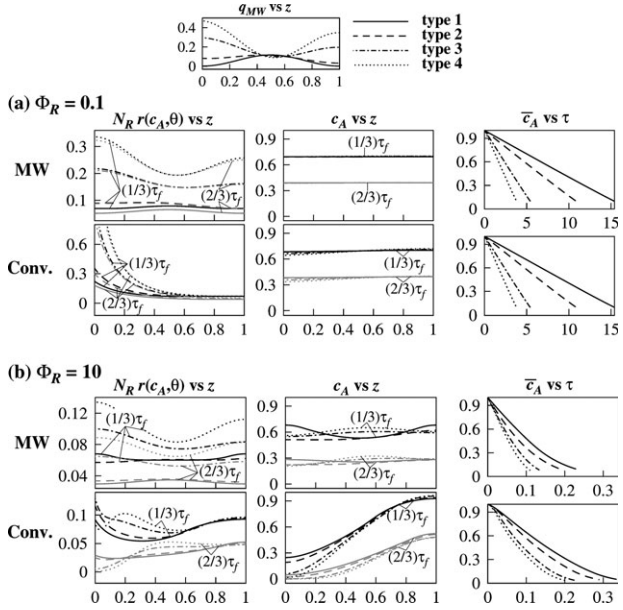

Figure 6. Spatial dynamics of reactor (shown at $\tau_f/3$ and $2\tau_f/3$ using darker and lighter shades, respectively) and overall reactor progress ($\bar{c}_A$ vs. τ) under microwave (MW) and conventional (Conv.) heating of Type 1–Type 4 configurations (solid, dash, dash-dotted, and dotted lines) in intermediate regime corresponding to $N_w = 0.5$, $f_p = 0.1$, and $f_w = 0.1$ for two limiting cases of $\Phi_R = 0.1$ and 10 in subplots (a) and (b), respectively.

intermediate regime of microwave heating. Source configuration strongly influences the reaction pattern at source specific resonating peaks ($N_w = n + 1/2$, $n = 0, 1, 2\ldots$), while reaction patterns are expected to remain almost invariant of source configuration at the common resonating location ($N_w = n$, $n = 1, 2..$). These features of reactor dynamics under intermediate regime of microwave heating are clearly reflected in the spatial heat requirement ($N_R r(c_A, \theta)$) of Figures 6 and 7, respectively. It may be observed from Figure 6 that Type 1 and Type 4 configurations lead to almost opposite reaction pattern at $N_w = 0.5$, where reaction fonts gradually shift from the center to walls from Type 1 to Type 4 configurations. On the other hand, reaction fonts appear almost at the same locations for all the configurations in Figure 7. Nevertheless, intermediate regime of microwave heating leads to much homogenized reaction and consequent reduction of concentration gradients compared to their conventional counterparts irrespective of either source configuration or reactor width (N_w) as may be observed from Figures 6 and 7. Obviously, the homogenization effect of intermediate regime of microwave heating becomes prominent in presence of mass transfer limitations $\Phi_R = 10$, where concentration gradients build up within the reactor following the individual heating pattern of microwave and conventional reactor. It may be noted from Figures 6 and 7 higher intensity of surface heating at $N_w = 1$ brings out the homogenization effect of microwave heating much more prominently than at $N_w = 0.5$. For the same reason, conventional reactor at $N_w = 1$ exhibits nonuniform reactant concentrations even at $\Phi_R = 0.1$, while concentration gradients are homogenized at $\Phi_R = 0.1$ for both the cases of microwave heating at $N_w = 0.5$ and 1 as well as conventional heating at $N_w = 0.5$ (Figures 6 and 7).

Extent of homogenization of reactor dynamics under microwave heating also relies on the intensity localized reaction in the conventional reactor, which is directly proportional to $\bar{q}_{MW}$. Thus, source configuration does influence the homogenization capacity of intermediate regime of microwave heating based on the magnitude of N_w with the influence to be much stronger at source specific resonating peaks ($N_w = n + 1/2$, $n = 0, 1\ldots$) compared to those at common resonating peaks ($N_w = n$, $n = 1, 2..$) according to the variations of $\bar{q}_{MW}$ from Type 1 to Type 4 configurations as discussed in "thin, intermediate, and thick regimes of microwave power absorption." Correspondingly, Figure 6b shows significantly greater homogenization of concentration gradients in Type 4 configuration of microwave heating with $\bar{q}_{MW} = 0.249$ compared to Type 1 configuration with $\bar{q}_{MW} = 0.06$. On the other hand, extent of homogenization under microwave heating remains much less influenced by source configuration at $N_w = 1$ (Figure 7b) as expected from the lower variation of $\bar{q}_{MW}$ from Type 1 to Type 4 configurations (changes from 0.741 to 0.607 from Type 1 to Type 4). Needless to mention that the influence of source configuration on reactor dynamics disappear in kinetically controlled regime as reflected in Figures 6a and 7a for $\Phi_R = 0.1$.

It follows that enhancement of reactor progress under microwave heating is much strongly influenced by source configuration at $N_w = 0.5$ compared to $N_w = 1$ as also reflected in the $\bar{c}_A$ vs. τ diagrams of Figures 6 and 7. Savings of reaction time in Type 1–Type 4 configurations of microwave heating at $N_w = 0.5$ and 1 are reported in Table 1, which shows that microwave heating at $N_w = 0.5$ reduces the reaction time by ≈46% in Type 4 configuration compared to

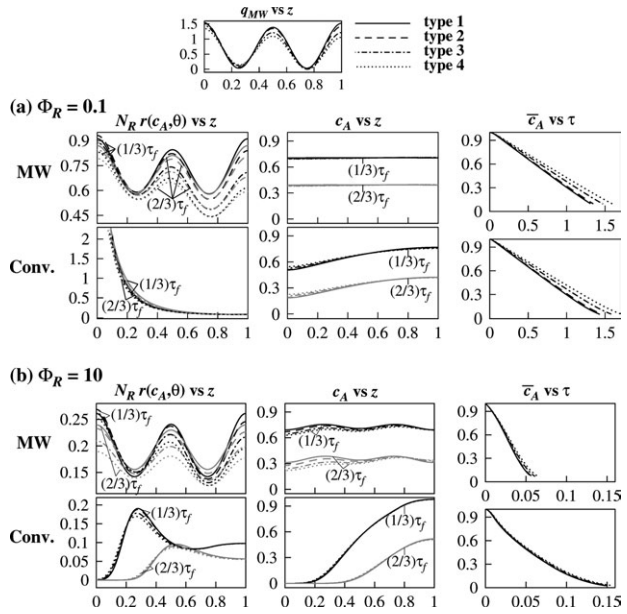

Figure 7. Spatial dynamics of reactor (shown at $\tau_f/3$ and $2\tau_f/3$ using darker and lighter shades, respectively) and overall reactor progress ($\bar{c}_A$ vs. τ) under microwave (MW) and conventional (Conv.) heating of Type 1–Type 4 configurations (solid, dash, dash-dotted, and dotted lines) in intermediate regime corresponding to $N_w = 1$, $f_p = 0.1$, and $f_w = 0.1$ for two limiting cases of $\Phi_R = 0.1$ and 10 in subplots (a) and (b), respectively.

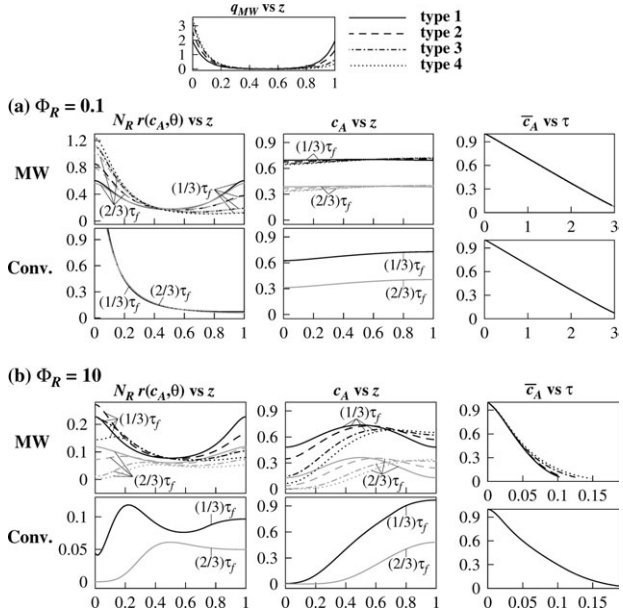

Figure 8. Spatial dynamics of reactor (shown at $\tau_f/3$ and $2\tau_f/3$ using darker and lighter shades, respectively) and overall reactor progress ($\bar{c}_A$ vs. τ) under microwave (MW) and conventional (Conv.) heating of Type 1–Type 4 configurations (solid, dash, dash-dotted, and dotted lines) in thick regime corresponding to $N_p = 6$, $f_p = 0.1$, and $f_w = 0.1$ for two limiting cases of $\Phi_R = 0.1$ and 10 in subplots (a) and (b), respectively.

much lower ≈31% savings of reaction time in Type 1 configuration for $\Phi_R = 10$. A opposite pattern is followed at $N_w = 1$, where Type 1 configuration of microwave heating causes higher savings of reaction time (≈64%) compared to Type 4 configuration (≈59%) although the variations are much smaller than those at $N_w = 0.5$ as expected. The above discussion reflects the nonlinear effect of source configuration in intermediate regime, where either one-sided or both sided source configuration can maximize the efficiency of microwave heating depending on reactor width (N_w). Also, selection of reactor width becomes a critical and nontrivial factor to maximize the efficiency of microwave heating due to its nonlinear influence on power absorption in intermediate regime.

Effect of microwave source configurations on microwave assisted and conventional reactor dynamics in thick regime of power absorption ($N_p = 6$)

Figure 8 illustrates the influence of source configuration on the dynamics of reactors in thick regime of microwave heating corresponding to $N_p = 6$, $f_p = 0.1$, $f_w = 0.1$ with subplots (a) and (b) illustrating the results for $\Phi_R = 0.1$ and 10, respectively. (Figure 8 also uses the same format as in previous figures with variations of the microwave heating pattern shown at the top.) The main feature that differentiates thick regime of reactors is the occurrence of reaction from and near the exposed surface/surfaces in both the modes of heating as reflected in the spatial profiles of $N_R r(c_A, \theta)$ of Figure 8. Nevertheless, microwave heating expands the reaction zone even in thick regime and hence homogenizes the dynamics of conventional reactor in presence of mass transfer limitations as can be seen from the concentration profiles of Figure 8b for $\Phi_R = 10$. However, homogenization of reactor dynamics is much lower in Type 4 configuration, where microwave heating resembles the heating pattern of conventional reactor. On the other hand, Type 1 configuration not only expands the reaction zone to both sides but also enhances the uniformity of reaction. Correspondingly, Type 1 configuration maximizes the homogenization capacity and consequent saving of reaction time of microwave heating in thick regime with significant enhancement from Type 4 configuration as illustrated in the c_A vs. z and $\bar{c}_A$ vs. τ diagrams of Figure 8b. Savings of reaction time for various configurations of microwave heating at $N_p = 6$ are also reported in Table 1. As in the previous cases, differences between the reactor dynamics under microwave and conventional heating disappear at $\Phi_R = 0.1$ as shown in Figure 8a.

Savings of reaction time under various configurations of microwave heating

To quantify the observed enhancement of reactor progress due to microwave heating in thin, intermediate, and thick regimes (Figures 5–8), we define percentage saving of reaction time under microwave heating as

$$\eta_{MW} = \left(1 - \frac{\tau_{f_{MW}}}{\tau_{f_{Conv}}}\right) \times 100. \tag{16}$$

Figure 9 illustrates the influence of source configuration on η_{MW} over the entire range of thin to thick regimes ($0.05 \le N_w \le 10$) with subplots (a)–(c) showing the influences at $\Phi_R = 0.1$, 1 and 10, respectively. It may be noted that results for intermediate Thiele modulus of $\Phi_R = 1$ is also included in Figure 9 to show significant savings of reaction time even at $\Phi_R = 1$. Here, solid, dashed, dash-dotted, and dotted lines in Figure 9 represent Type 1, Type 2, Type 3, and Type 4 configurations, respectively. All other parameters in Figure 9 correspond to those in Figures 5–8.

Figure 9 quantifies the facts observed in Figures 5–8 that enhancement of reactor progress due to microwave heating results from the transport limitations within the reactor. At $\Phi_R = 0.1$, where mass transfer does not limit the progress of

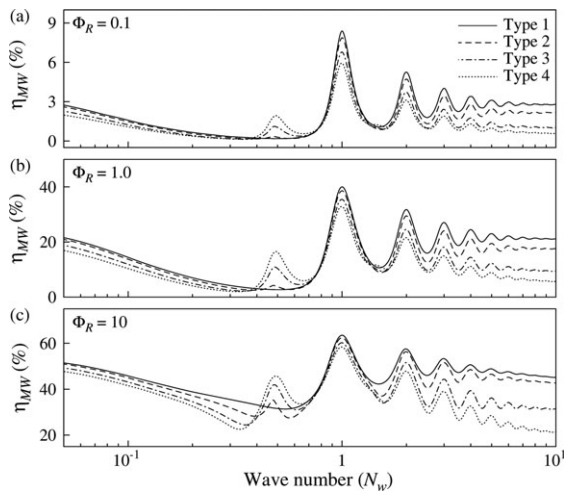

Figure 9. Effect of source configuration on η_{MW} over the entire range of $0.05 \le N_w \le 10$ spanning thin, intermediate, and thick regimes for Type 1–Type 4 configurations (solid, dash, dash-dotted, and dotted lines) with $f_p = 0.1$, $f_w = 0.1$, and $\Phi_R = 0.1$, 1 and 10 in subplots (a), (b), and (c), respectively.

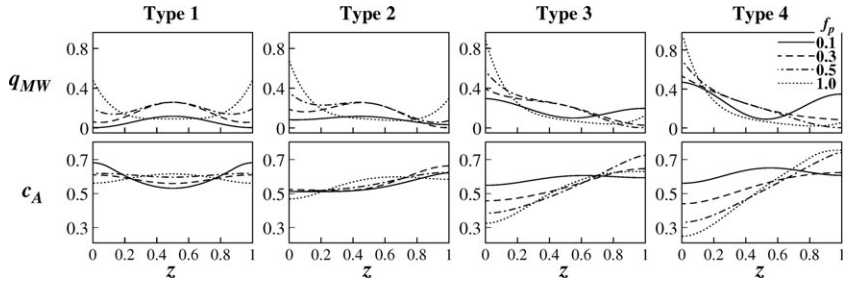

Figure 10. Effect of f_p on power absorption pattern (q_{MW}) and homogeneity of reactant concentration under Type 1–Type 4 configurations of microwave heating (shown at $\tau_f/3$) at $N_w = 0.5$, $f_w = 0.1$, and $\Phi_R = 10$ with solid, dash, dash-dotted, and dotted lines representing $f_p = 0.1$, 0.3, 0.5, and 1, respectively.

reactor, savings of reaction time can be observed to be practically low in most of the regions except around $N_w = 1$. Savings of reaction time become prominent at $\Phi_R = 1$ and become significantly high as Φ_R increases to 10 representing high mass transfer limitations within the reactor. Figure 9 also establishes one-to-one correlation between η_{MW} and intensity of surface heating or $\bar{q}_{MW}$, observed in the dynamics of selected reactor dimensions in Figures 5–8, for the entire range of thin to thick regimes. Thus, variations of $\bar{q}_{MW}$ with N_w can be used for apriori prediction of the nontrivial variations of η_{MW} with reactor dimension especially in intermediate regime. The master curves provided in Figure 9 can be used for quick and easy estimation of the appropriate reactor dimension to attain maximum savings of reaction time. For example, savings of reaction time can be maximized by operating reactor at the resonating locations of $\bar{q}_{MW}$ ($N_w = 1, 2\ldots$) as can be easily seen from Figure 9. It may be noted that decrease of η_{MW} with N_w in thick regime of microwave heating is due to shrinking penetration of microwave as discussed before and $\eta_{MW} \to 0$ in the limit of $N_p \to \infty$.

Figure 9 also extends the influence of source configuration on η_{MW} over the entire range of *thin* to *thick* regimes as discussed in previous sections for few specific N_w's. It is evident from Figure 9 that progress of reactor in *thin* and *thick* regimes of microwave heating can be sequentially enhanced by selecting type 1 configurations over type 2, type 3 and type 4 configurations, where the effect is more pronounced in *thick* regime as can be expected from the previous discussions. Higher savings of reaction time in type 1 configuration than type 4 configuration is solely driven by higher intensity of heating ($\bar{q}_{MW}$) in *thin* regime of microwave heating. On the other hand, difference in spatial power absorption pattern drives the difference in η_{MW} from type 1 to type 4 configurations in *thick* regime of microwave heating. In contrast, both power absorption pattern as well as intensity of $\bar{q}_{MW}$ drive the enhanced dynamics in *intermediate* regime and causes the optimum section of source configuration to be highly nontrivial as illustrated before for $N_w = 0.5$ and 1. It may be noted that two completely opposite source configurations optimize the efficiency of microwave heating at $N_w = 0.5$ and 1 (type 4 and type 1, respectively). In such cases, the master curves provided in Figure 9 become extremely useful to select appropriate microwave source configuration for a given reactor dimension (N_w).

Effect of f_p *on efficiency of reactor under microwave heating*

Parameter f_p determines the probability of resonances in power absorption and consequent span of *intermediate* regime, where resonances occur if $f_p \leq 1.5/\pi$.[37] For $f_p > 1.5/\pi$, power absorption directly transform from uniform distributions of *thin* regime to exponentially decaying profiles of *thick* regimes without undergoing resonances. Correspondingly, resonating power absorption patterns of *intermediate* regime at $f_p = 0.1$ gradually transform into the exponentially decaying profiles as f_p increases beyond $1.5/\pi$ even at $N_w \approx 0.5$. This is reflected in Figure 10, which shows the above transformation of spatial profiles of q_{MW} at $N_w = 0.5$ and $f_w = 0.1$ as f_p increases from 0.1 (solid lines) to 0.3 (dash lines), 0.5 (dash-dotted lines) and 1 (dotted lines) for type 1 to type 4 configurations. It may be noted that f_p is always bound by 1 $\left(0 \leq f_p \leq 1\right)$ according to the definitions of λ_{eff} and $D_{p_{eff}}$ (see Eq. A1). Associated changes in the homogenization of concentration gradients under microwave heating in presence of mass transfer limitations at $\Phi_R = 10$ are also shown in Figure 10 at $\tau = \tau_f/3$. It may be observed from Figure 10 that transformation from volumetric to highly one sided heating for predominantly one sided incidences of Type 3 and Type 4 configurations significantly hampers the homogenization ability of microwave heating from $f_p = 0.1$ to 1. Accordingly, η_{MW} reduces by ≈16% and 27% from $f_p = 0.1$ to 1 for Type 3 and Type 4 configurations, respectively, as may be calculated from the listed values of $\bar{q}_{MW}$ and η_{MW} with f_p in Table 2. It is important to note that effect of the changes in power distribution patterns from $f_p = 0.1$ to 1 dominate over the variations of $\bar{q}_{MW}$ for Type 3 and Type 4 configurations. On the other hand, alterations of heating pattern from $f_p = 0.1$ to 1 do not alter the homogenization capacity of microwave heating significantly in case of evenly distributed incidences of Type 1 and Type 2 configurations, where reactions occur from both sides even at $f_p = 1$ (Figure 10). In such cases, influence of f_p on the efficiency of microwave heating to reduce processing time mainly depends on the variations of $\bar{q}_{MW}$. Accordingly, Table 2 shows higher η_{MW} at $f_p = 1$ compared to those at $f_p = 0.1$ following the variations of $\bar{q}_{MW}$ for Type 1 and Type 2 configurations. It may be noted that nonmonotonic variations of $\bar{q}_{MW}$ for Type 1 configuration is also reflected in the nonmonotonic changes in η_{MW} from $f_p = 0.1$ to 1.

Table 2. Variations of $\bar{q}_{MW}$ and η_{MW} with f_p for $N_w = 0.5$, $f_w = 0.1$, and $\Phi_R = 10$

	Type 1		Type 2		Type 3		Type 4	
f_p	$\bar{q}_{MW}$	η_{MW}	$\bar{q}_{MW}$	η_{MW}	$\bar{q}_{MW}$	η_{MW}	$\bar{q}_{MW}$	η_{MW}
0.1	0.06	31.56	0.09	32.61	0.17	40.84	0.25	45.50
0.3	0.15	40.10	0.16	33.94	0.20	32.58	0.24	34.68
0.5	0.19	44.03	0.20	35.95	0.21	28.25	0.23	26.29
1	0.17	41.40	0.17	36.26	0.17	25.33	0.17	18.5

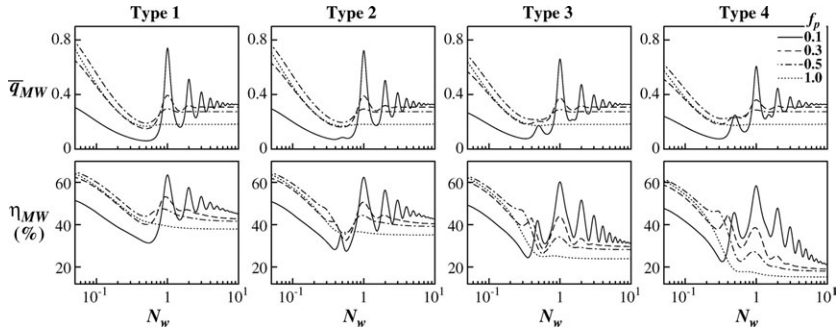

Figure 11. Effect of f_p on $\bar{q}_{MW}$ and η_{MW} for Type 1–Type 4 configurations over the entire range of thin to thick regimes $(0.05 \leq N_w \leq 10)$ at $f_w = 0.1$ and $\Phi_R = 10$.

Solid, dash, dash-dotted, and dotted lines represent $f_p = 0.1$, 0.3, 0.5, and 1, respectively.

It follows from Table 2 that variations of $\bar{q}_{MW}$ with f_p does not follow a specific pattern and may either be increasing or decreasing depending on source configuration as well as other propagation parameters. As higher $\bar{q}_{MW}$ enhances η_{MW} while lower $\bar{q}_{MW}$ suppresses η_{MW}, influence of the variations of $\bar{q}_{MW}$ from $f_p = 0.1$ to 1 on η_{MW} may or may not follow the negative influence of the transformation of power absorption pattern toward surface heating. Correspondingly, efficiency of microwave heating may or may not follow the variations of $\bar{q}_{MW}$ with f_p depending on the relative contributions from the variations of power absorption pattern and intensity of power absorption ($\bar{q}_{MW}$). This fact is established in Figure 11, which shows the variations of $\bar{q}_{MW}$ and η_{MW} with f_p over the entire range of $0.05 \leq N_w \leq 10$ for Type 1 to Type 4 configurations. Figure 11 shows the results for $f_w = 0.1$ and $\Phi_R = 10$ with solid, dash, dash-dotted, and dotted lines representing $f_p = 0.1$, 0.3, 0.5, and 1, respectively. As stated at the beginning of this section, resonating intermediate regime of power absorption gradually disappear for all the configurations as f_p increases from 0.1 to 1 in Figure 11. It may be noted that variations of η_{MW} follow a one-to-one correspondence with those of $\bar{q}_{MW}$ in thick regime as well at the common resonating locations ($N_w = 1, 2\ldots$), where $\bar{q}_{MW}$ decreases monotonically from $f_p = 0.1$ to 1 and inflicts similar influences on η_{MW} as the transformation of power distribution patterns. Variations of η_{MW} also show a one-to-one correspondence with $\bar{q}_{MW}$ in thin regime, where effect of variations of $\bar{q}_{MW}$ dominate over other changes. On the other hand, influence of power absorption pattern dominate at source specific resonating location of $N_w = 0.5$ and 1.5 for highly one sided Type 3 and Type 4 configuration and η_{MW} shows a monotonic decrease from $f_p = 0.1$ to 1 irrespective of the variations of $\bar{q}_{MW}$. It may be noted that higher resemblance between microwave and conventional heating at $f_p = 1$ causes much greater reduction of η_{MW} from $f_p = 0.1$ to 1 in intermediate regime for highly one-sided type 4 configuration than other configurations.

Effect of f_w on efficiency of reactor under microwave heating

Parameter f_w controls the scattering of electromagnetic wave at the sample boundaries via Eq. 12 and hence alters the transmitted and reflected fields within the sample. This influences the resulting electric field and associated heating patterns, where effects are much nonlinear/nontrivial compared to the effect of f_p. Unlike f_p, variations of power absorption with f_w do not follow a specific pattern and depend strongly on sample width and source configuration in addition to other propagation parameters as illustrated in Figure 12 for three different sample thickness in intermediate regime corresponding to $N_w = 0.5$, 1, and 1.5. Parameter f_w is also bound by 1 $(0 \leq f_w \leq 1)$ as wavelength of microwave is maximum in vacuum or free space and Figure 12 shows the variations of power absorption patterns as f_w increases from 0.1 (solid lines) to 0.5 (dash lines), 0.7 (dash-dotted lines), and 1 (dotted line) for Type 1–Type 4 configurations at $f_p = 0.1$. Figure 12 shows that although f_w alters the power absorption patterns depending on source configuration and reactor width, volumetric nature of microwave heating in intermediate regime remains unaltered from $f_w = 0.1$ to 1.

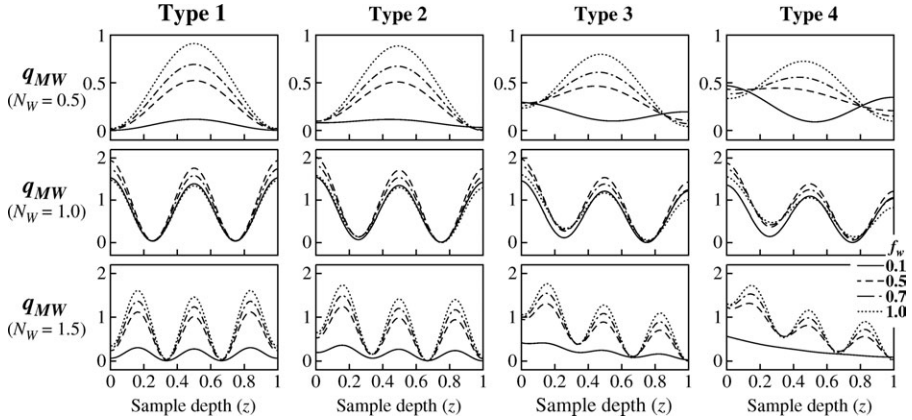

Figure 12. Effect of f_w on power absorption patterns at $N_w = 0.5$, 1, 1.5, and $f_p = 0.1$ with solid, dash, dash-dotted, and dotted lines representing $f_w = 0.1$, 0.5, 0.7, and 1, respectively.

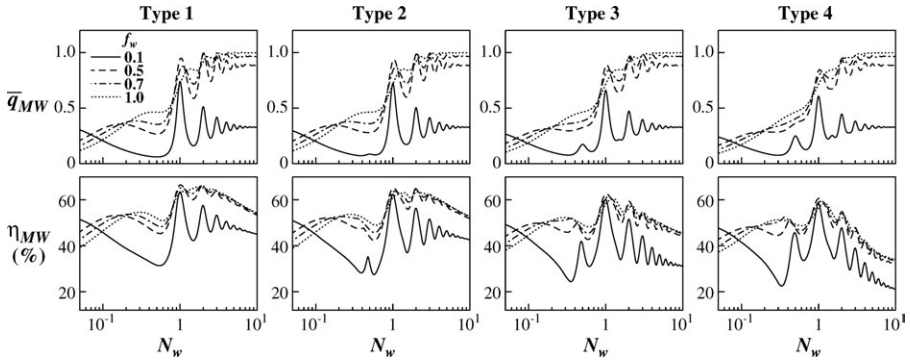

Figure 13. Effect of f_w on $\bar{q}_{MW}$ and η_{MW} for Type 1 to Type 4 configurations over the entire range of thin to thick regimes $(0.05 \leq N_w \leq 10)$ at $f_p = 0.1$ and $\Phi_R = 10$.

Solid, dash, dash-dotted, and dotted lines represent $f_w = 0.1$, 0.5, 0.7, and 1, respectively.

The same is also true for thin regime and not shown here. Consequently, variations of η_{MW} with f_w show one-to-one correspondence for all the configurations as shown in Figure 13 for the entire range of $0.05 \leq N_w \leq 10$. Figure 13 shows the results for $\Phi_R = 10$ with other parameters to be same as in Figure 12. It may be noted that higher intensity of $\bar{q}_{MW}$ increases η_{MW} from $f_w = 0.1$ to 1 for most of the regions expect a very small region of thin regime ($N_w \lessapprox 0.07$).

Conclusive Remarks

This work presents a detailed analysis on the role of microwave heating strategies in optimizing the progress of a first-order endothermic reaction occurring in a semi-infinite batch reactor. Here, microwave heating strategies are analyzed in terms of different intensities of incident radiations from left and right sides of the reactor. Four different configurations are considered such that they represent the entire spectrum of possible arrangement of microwave sources spanning uniform intensities of radiations from both sides to highly localized incidences from one side. In all the cases, total input power is kept constant by maintaining same total intensities of radiations from left and right sides. The analysis has been performed by considering detail description of microwave propagation via Helmholtz equation, which is solved with coupled energy and mass balance equations to simulate the progress of reactor under various configurations of microwave heating. Simulated progress of reactor under various configurations of microwave heating are then compared in terms of the extent of changes in concentration gradients and reaction time compared to those under conventional heating, where comparison is done for all the possible microwave heating patterns spanning thin to thick regimes.

This work shows that source configuration plays a critical role in enhancing the efficiency of microwave heating to homogenize reactor dynamics and reduce reaction time of conventional heating. Evenly distributed incidences from both sides promote the efficiency of microwave heating in thin and thick regimes of microwave heating. On the other hand, either one sided or distributed incidences may enhance efficiency of microwave heating in intermediate regime depending on reactor dimension. Correspondingly, efficiency of microwave heating has been quantified by providing percentage savings of reaction time $[\eta_{MW} = (1 - \tau_{f_{MW}}/\tau_{f_{Conv}}) \times 100]$ over the entire range of thin to thick regimes for all the four source configurations. These master curves (η_{MW} vs. N_w) clearly illustrate critical role of source configuration in maximizing η_{MW} in various regimes of microwave heating and can be extremely useful to select optimum source configuration for given reactor dimension (especially in intermediate regime). Master curves have also been provided for varying f_p and f_w, which reveal nontrivial choice of optimum source configuration for reactors with packings of different dielectric properties.

Although numerous experiments have been conducted in past to show enhanced progress of reaction in presence of microwave heating, neither of them considered variations of microwave heating strategies. This may be due to intricate design involved with various heating strategies as well as their complicated/nontrivial effect on microwave power absorption. Thus, prior knowledge about the effect of targeted microwave configurations on the local as well as overall reactor progress are necessary for successful design of experimental set up. This work provides the background knowledge on the probable effect of various possible microwave heating strategies on the progress of reactors of various dimensions/properties and, thus, may form the basis for set up of systematic and designed experiments in future.

Acknowledgments

The authors would like to thank the editor and anonymous reviewers for their critical comments, which helped to improve the quality and readability of the manuscript.

Notation

C_A = reactant concentration, mol m^{-3}
C_{A_0} = initial reactant concentration, mol m^{-3}
c_A = dimensionless reactant concentration
$\bar{c}_A$ = dimensionless average concentration
$(\rho C_p)_{eff}$ = effective heat capacity, J m^{-3} K^{-1}
$D_{p_{eff}}$ = effective penetration depth, m
E = activation energy, kJ kmol^{-1}
E_x = dimensionless electric field (scaled with $\sqrt{2I_0/2\varepsilon_0}$) within the sample
E_f = dimensionless electric field (scaled with $\sqrt{2I_0/2\varepsilon_0}$) within free space
F = frequency, Hz
f_p = ratio of λ_{eff} to $2\pi D_{p_{eff}}$
f_w = ratio of λ_{eff} to λ_0
I_0 = total intensity of incident radiation, W m^{-2}
I_L = intensity of incident radiation from left, W m^{-2}
I_R = intensity of incident radiation from right, W m^{-2}
k_{eff} = effective thermal conductivity, W m^{-1} K^{-1}
L = half-width of packed column, m
N_p = penetration number $\left(=\frac{2L}{D_{p_{eff}}}\right)$
N_w = wave number $\left(=\frac{2L}{\lambda_{eff}}\right)$
N_R = heat-reaction number $\left(=\frac{2L\Delta H_R \phi R(C_{A_0},T_0)}{I_0}\right)$

Q_{MW} = absorbed power distribution, W m^{-3}
q_{MW} = dimensionless absorbed power distribution
$\bar{q}_{MW}$ = dimensionless average absorbed power
t = time, s
T = temperature, K
T_0 = initial temperature, K
v_x = dimensionless real field component
w_x = dimensionless imaginary field component
Z = distance, m
z = dimensionless distance

Greek letters

α_{eff} = effective thermal conductivity $\left(=\frac{k_{eff}}{(\rho C_p)_{eff}}\right)$
β = conduction number $\left(=\frac{k_{eff}T_0}{2LI_0}\right)$
ΔH = Heat of reaction, J mol^{-1}
γ_R = dimensionless activation energy $\left(=\frac{E}{RT_0}\right)$
ε_0 = free space permittivity, Farad m^{-1}
θ = dimensionless temperature
$\bar{\theta}$ = average Temperature
κ'_{eff} = effective dielectric constant
κ''_{eff} = effective dielectric loss
λ_{eff} = effective wavelength of microwave within packed bed, m
λ_0 = wavelength within free space, m
ρ = density, kg m^{-3}
τ = dimensionless time
τ_D = diffusion number $\left(=\frac{\phi\alpha_{eff}}{D_{eff}}\right)$
τ_f = dimensionless reaction time
$\tau_{f_{MW}}$ = dimensionless reaction time in microwave assisted reactor
$\tau_{f_{Conv}}$ = dimensionless reaction time in conventional reactor
θ = dimensionless temperature $\left(=\frac{k_{eff}(T-T_0)}{2LI_0}\right)$
ϕ = porosity
Φ_R = Thiele Modulus $\left(=\frac{4L^2\phi R(C_{A_0},T_0)}{D_{eff}C_{A_0}}\right)$

Literature Cited

1. Balanis CA. *Advanced Engineering Electromagnetics*. New York: Wiley, 1989.
2. Vadivambal R, Jayas DS. Non-uniform temperature distribution during microwave heating of food materials—a review. *Food Bioprocess Technol*. 2010;3:161–171.
3. Kharissova OV, Kharisov BI, Valdes JJR. Review: the use of microwave irradiation in the processing of glasses and their composites. *Ind Eng Chem Res*. 2010;49:1457–1466.
4. Mutyala S, Fairbridge C, Pare JRJ, Belanger JMR, Ng S, Hawkins R. Microwave applications to oil sands and petroleum: a review. *Fuel Process Technol*. 2010;91:127–135.
5. Zhang M, Tang J, Mujumdar AS, Wang S. Trends in microwave-related drying of fruits and vegetables. *Trends Food Sci Technol*. 2006;17:524–534.
6. Kingman SW. Recent developments in microwave processing of minerals. *Int Mater Rev*. 2006;51:1–12.
7. Icier F, Baysal T. Dielectrical properties of food materials—1: factors affecting and industrial uses. *Crit Rev Food Sci*. 2004;44:465–471.
8. Jones DA, Lelyveld TP, Mavrofidis SD, Kingman SW, Miles NJ. Microwave heating applications in environmental engineering—a review. *Resour Conserv Recy*. 2002;34:75–90.
9. Sumnu G. A review on microwave baking of foods. *Int J Food Sci Technol*. 2001;36:117–127.
10. Haque KE. Microwave energy for mineral treatment processes—a brief review. *Int J Miner Process*. 1999;57:1–24.
11. Clark DE, Sutton WH. Microwave processing of materials. *Annu Rev Mater Sci*. 1996;26:299–331.
12. Ayappa KG. Modelling transport processes during microwave heating: a review. *Rev Chem Eng*. 1997;13:1–69.
13. Osepchuk JM. A history of microwave-heating applications. *IEEE Trans Microwave Theory*. 1984;32:1200–1224.
14. Leonelli C, Mason TJ. Microwave and ultrasonic processing: now a realistic option for industry. *Chem Eng Process*. 2010;49:885–900.
15. Lin CC, Guo GL, Tsai TL. A bi-order kinetic model for poly(methyl methacrylate) decomposition in HNO3 using microwave irradiation. *AIChE J*. 2009;55:2150–2158.
16. Strauss CR, Rooney DW. Accounting for clean, fast and high yielding reactions under microwave conditions. *Green Chem*. 2010;12:1340–1344.
17. Durka T, Van Gerven T, Stankiewicz A. Microwaves in heterogeneous gas-phase catalysis: experimental and numerical approaches. *Chem Eng Technol*. 2009;32:1301–1312.
18. Polshettiwar V, Nadagouda MN, Varma RS. Microwave-assisted chemistry: a rapid and sustainable route to synthesis of organics and nanomaterials. *Aust J Chem*. 2009;62:16–26.
19. Cherbanski R, Molga E. Intensification of desorption processes by use of microwaves—an overview of possible applications and industrial perspectives. *Chem Eng Process*. 2009;48:48–58.
20. Kappe CO. Microwave dielectric heating in synthetic organic chemistry. *Chem Soc Rev*. 2008;37:1127–1139.
21. Bowman MD, Holcomb JL, Kormos CM, Leadbeater NE, Williams VA. Approaches for scale-up of microwave-promoted reactions. *Org Process Res Dev*. 2008;12:41–57.
22. Baxendale IR, Hayward JJ, Ley SV. Microwave reactions under continuous flow conditions. *Combin Chem High Throughout Scr*. 2007;10:802–836.
23. Cecilia R, Kunz U, Turek T. Possibilities of process intensification using microwaves applied to catalytic microreactors. *Chem Eng Process*. 2007;46:870–881.
24. Zhang XL, Hayward DO. Applications of microwave dielectric heating in environment-related heterogeneous gas-phase catalytic systems. *Inorg Chim Acta*. 2006;359:3421–3433.
25. Tokuyama H, Nakamura M. Acceleration of reaction by microwave irradiation. *J Syn Org Chem Jpn*. 2005;63:523–538.
26. de la Hoz A, Diaz-Ortiz A, Moreno A. Microwaves in organic synthesis. Thermal and non-thermal microwave effects. *Chem Soc Rev*. 2005;34:164–178.
27. Nuchter M, Ondruschka B, Bonrath W, Gum A. Microwave assisted synthesis—a critical technology overview. *Green Chem*. 2004;6:128–141.
28. Nuchter M, Muller U, Ondruschka B, Tied A, Lautenschlager W. Microwave-assisted chemical reactions. *Chem Eng Technol*. 2003;26:1207–1216.
29. Lidstrom P, Tierney J, Wathey B, Westman J. Microwave assisted organic synthesis—a review. *Tetrahedron*. 2001;57:9225–9283.
30. Caddick S. Microwave-assisted organic-reactions. *Tetrahedron*. 1995;51:10403–10432.
31. Abramovitch RA, Applications of microwave-energy in organic-chemistry—a review. *Org Prep Proced Int*. 1991;23:685–711.
32. Stuerga D, Gaillard P. Microwave heating as a new way to induce localized enhancements of reaction rate. Non-isothermal and heterogeneous kinetics. *Tetrahedron*. 1996;52:5505–5510.
33. Toukoniitty B, Warna J, Mikkola JP, Helle M, Saxen H, Murzin DY, Salmi T. Modelling of enantioselective and racemic hydrogenation of ethyl pyruvate on a Pt/Al2O3 catalyst in the presence of microwave irradiation. *Chem Eng Process*. 2009;48:837–845.
34. Carta R, Loddo L. Effect of temperature and microwave power on the hydrolysis of phenyl acetate. *AIChE J*. 2004;50:1523–1529.
35. Ayappa KG, Davis HT, Crapiste G, Davis EA, Gordon J. Microwave heating: an evaluation of power formulations. *Chem Eng Sci*. 1991;46:1005–1016.
36. Basak T, Kumaran SS. A generalized analysis on material invariant characteristics for microwave heating of slabs. *Chem Eng Sci*. 2005;60:5480–5498.
37. Bhattacharya M, Basak T. New closed form analysis of resonances in microwave power for material processing. *AIChE J*. 2006;52:3707–3721.
38. Bhattacharya M, Basak T. Detailed material-invariant analysis on spatial resonances of power absorption for microwave-assisted material processing with distributed sources. *Ind Eng Chem Res*. 2007;46:750–760.
39. Bhattacharya M, Basak T. Generalized scaling on forecasting heating patterns for microwave processing. *AIChE J*. 2008;54:56–73.
40. Stuerga DAC, Gaillard P. Microwave athermal effects in chemistry: a myth's autopsy.2. Orienting effects and thermodynamic consequences of electric field. *J Microwave Power Electromagn Energy*. 1996;31:101–113.
41. Herrero MA, Kremsner JM, Kappe CO. Nonthermal microwave effects revisited: on the importance of internal temperature monitoring and agitation in microwave chemistry. *J Org Chem*. 2008;73:36–47.
42. Yeo YK, Kim HY, Kim IW, Moon I, Chung Y, Levdansky VV. Analysis of catalytic reaction systems under microwaves to save energy. *Korean J Chem Eng*. 2003;20;1–7.

43. Perry WL, Datye AK, Prinja AK, Brown LF, Microwave heating of endothermic catalytic reactions: Reforming of methanol. *AIChE J*. 2002;48:820–831.
44. Shin GI, Yeo YK, Jo BY, Kim HY, Levdansky VV. Analysis on effects of microwave heating in porous catalysts. *J Chem Eng Jpn*. 2001;34:1567–1574.
45. Pipus G, Plazl I, Koloini T. Esterification of benzoic acid in microwave tubular flow reactor. *Chem Eng J*. 2000;76:239–245.
46. Plazl I, Pipus G, Koloini T. Microwave heating of the continuous flow catalytic reactor in a nonuniform electric field. *AIChE J*. 1997;43:754–760.
47. Bhattacharya M, Basak T, Senagala R. A comprehensive theoretical analysis for the effect of microwave heating on the progress of a first order endothermic reaction. *Chem Eng Sci*. 2011;66:5832–5851.
48. Basak T, Aparna K, Meenakshi A, Balakrishnan AR. Effect of ceramic supports on microwave processing of porous food samples. *Int J Heat Mass Transfer*. 2006;49:4325–4339.
49. Zhang Q, Jackson TH, Ungan A, Gao D. Numerical modeling of continuous hybrid heating of cryo-preserved tissue. *Int J Heat Mass Transfer*. 1999;42:395–403.
50. Zhang QO, Jackson TH, Ungan A. Numerical modeling of microwave induced natural convection. *Int J Heat Mass Transfer*. 2000;43:2141–2154.
51. Cha-um W, Rattanadecho P, Pakdee W. Experimental and numerical analysis of microwave heating of water and oil using a rectangular wave guide: influence of sample sizes, positions, and microwave power. *Food Bioprocess Technol*. 2011;4:544–558.
52. Rattanadecho P. The simulation of microwave heating of wood using a rectangular wave guide: Influence of frequency and sample size. *Chem Eng Sci*. 2006;61:4798–4811.
53. Ayappa KG, Davis HT, Davis EA, Gordon J. Analysis of microwave-heating of materials with temperature-dependent properties. *AIChE J*. 1991;37:313–322.
54. Bhattacharya M, Basak T. Linear stability analysis for the onset of convection during microwave heating of oil confined within horizontal plates. *J Appl Phys*. 2009;105:Art No 024906
55. Bhattacharya M, Basak T. On the analysis of microwave power and heating characteristics for food processing: asymptotes and resonances. *Food Res Int*. 2006;39:1046–1057.
56. Bhattacharya M, Basak T, Ayappa KG. A fixed grid finite element based enthalpy formulation for generalized phase change problems: role of superficial mushy region. *Int J Heat Mass Transfer*. 2002;45:4881–4898.
57. Reddy JN. *An Introduction to Finite Element Method*. New York:Mc Graw-Hill, 1993.
58. Fricke H. The Complex conductivity of a suspension of stratified particles of spherical or cylindrical form. *J Phys Chem*. 1955;59: 168–170.

Appendix A: Expression for Effective Dielectric Properties of Packed Bed

Effective wavelength and penetration depth within a domain with dielectric packings be obtained from the effective dielectric constant ($\kappa_{\text{eff}}^{'}$) and dielectric loss ($\kappa_{\text{eff}}^{''}$) as

$$\lambda_{\text{eff}} = \frac{c\sqrt{2}}{f\sqrt{\sqrt{\kappa_{\text{eff}}^{\prime 2} + \kappa_{\text{eff}}^{\prime\prime 2}} + \kappa_{\text{eff}}^{\prime}}} \tag{A1a}$$

$$D_{p_{\text{eff}}} = \frac{c}{\sqrt{2}\pi f}\frac{1}{\sqrt{\sqrt{\kappa_{\text{eff}}^{\prime 2} + \kappa_{\text{eff}}^{\prime\prime 2}} - \kappa_{\text{eff}}^{\prime}}}. \tag{A1b}$$

Here f is the frequency of incident microwave radiation. The effective dielectric properties ($\kappa_{\text{eff}}^{'}$ and $\kappa_{\text{eff}}^{''}$) in turn depend on dielectric properties of the packing and the porosity/dispersity of the column. Based on the literature,[58] an unified expression for $\kappa_{\text{eff}}^{'}$ and $\kappa_{\text{eff}}^{''}$ can be written as

$$\kappa_{\text{eff}}^{\prime} + i\kappa_{\text{eff}}^{\prime\prime} = \frac{(\kappa_{\text{p}}^{\prime *} + i\kappa_{\text{p}}^{\prime\prime *})[1 + a\phi + a(\kappa_{\text{p}}^{\prime *} + i\kappa_{\text{p}}^{\prime\prime *})(1-\phi)]}{1 - \phi + (\kappa_{\text{p}}^{\prime *} + i\kappa_{\text{p}}^{\prime\prime *})(a + \phi)} \tag{A2}$$

where $\kappa_{\text{p}}^{\prime}*$ and $\kappa_{\text{p}}^{\prime\prime}*$ are the dielectric constant and dielectric loss of packing, ϕ is the porosity, and $a = 2$ or 1 depending on whether packing are spherical or cylindrical, respectively. Equation A.2 uses the fact that dielectric constant and dielectric loss of free space are given by 1 and 0, respectively. This in turn results in the following definition of wave length within free space (λ_0)

$$\lambda_0 = \frac{c}{f}, \tag{A3}$$

which follows from Eq. A1a.

Appendix B: Analytical Solution of Microwave-Induced Heat Source Distribution (q_{MW}) for Constant Dielectric Properties

Expressions for C_1^n–C_4^n and C^d in terms of N_{w}, f_{w}, f_{p} and microwave source configuration (I_{L}/I_0 and I_{R}/I_0) are given by

$$C_1^n = c_2\cosh(2\pi N_{\text{w}} f_{\text{p}}) + c_4\sinh(2\pi N_{\text{w}} f_{\text{p}}) + 2\sqrt{\frac{I_{\text{L}} I_{\text{R}}}{I_0^2}}[c_1\cos(2\pi N_{\text{w}}) + c_3\sin(2\pi N_{\text{w}})] \tag{B1a}$$

$$C_2^n = \left(1 - 2\frac{I_L}{I_0}\right)\left[c_2\sinh(2\pi N_{\text{w}} f_{\text{p}}) + c_4\cosh(2\pi N_{\text{w}} f_{\text{p}})\right] \tag{B1b}$$

$$C_3^n = c_1\cos(2\pi N_{\text{w}}) + c_3\sin(2\pi N_{\text{w}}) + 2\sqrt{\frac{I_{\text{L}} I_{\text{R}}}{I_0^2}}\left[c_2\cosh(2\pi N_{\text{w}} f_{\text{p}}) + c_4\sinh(2\pi N_{\text{w}} f_{\text{p}})\right] \tag{B1c}$$

$$C_4^n = -\left(1 - 2\frac{I_{\text{L}}}{I_0}\right)[c_1\sin(2\pi N_{\text{w}}) - c_3\cos(2\pi N_{\text{w}})] \tag{B1d}$$

$$C^d = \left(c_3^2 - c_1^2\right)\cos(4\pi N_{\text{w}}) + \left(c_2^2 + c_4^2\right)\cosh(4\pi N_{\text{w}} f_{\text{p}}) - 2c_1c_3\sin(4\pi N_{\text{w}}) + 2c_2c_4\sinh(4\pi N_{\text{w}} f_{\text{p}}) \tag{B1e}$$

with

$$c_1 = 1 + f_p^2 - f_w^2, \tag{B2a}$$

$$c_2 = 1 + f_p^2 + f_w^2, \tag{B2b}$$

$$c_3 = -2f_p f_w, \tag{B2c}$$

$$c_4 = 2f_w. \tag{B2d}$$

Manuscript received Jan. 16, 2012, revision received Mar. 26, 2012, and final revision received May 14, 2012.